RSC Advances

ROYAL SOCIETY OF CHEMISTRY

www.rsc.org/advances

An axisymmetric model for the analysis of dynamic surface tension

S.I. Arias[a], J.R. Fernández[b], L. García-Rio[c*], J.C. Mejuto[a], M.C. Muñiz[d] and C. Núñez[e]

A quantitative treatment of dynamic surface tension data has been carried out with different mathematical approaches taking into account a difusion-controlled mechanism. The classical model has been modified in order to achieve a better description of the experimental conditions by considering a finite diffusion domain. The domain has been fixed keeping the restriction that the surfactant concentration in this region should remain constant after the adsorption at the air-water interface, in such a way that the number of surfactant unimers is 30 times the number adsorbed at the interface. The finite diffusion restriction has been used both in 1D and axisymmetric models, the latter one being the most accurate and needing a smaller diffusion domain since it considers surfactant adsorption at a sphere resembling the physical experiments. A distorted sphere geometry taking into account the Laplace-Young equation has also been studied.

1 Introduction

Dynamic surface tension at the air/water interface is an important property in a wide scope of phenomena, like wetting, flotation and sedimentation among others. It plays a major role in several applications like foam production, film creation and coatings, filtration and cleaning processes [1–3].

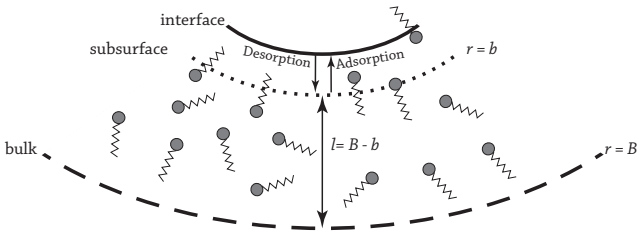

Fig. 1 Subsurface and air/water interface

When a new air/water interface is created, the surface concentration of unimers is less than at equilibrium, deriving in a flow of unimers from the bulk solution to the interface. This flow causes a drop in the surface tension in order to reach its equilibrium value[4]. This process can last from milliseconds to hours or even days, and the time taken depends mainly on the velocity of diffusion from the bulk solution to the so-called subsurface —i.e. an hypothetical layer located a few nanometers beneath the interface, see fig. 1— plus the total time taken in moving between the subsurface and the interface. If we initially consider an empty interface, unimers travel a diffusion length denoted by l, see fig.1, and then they are directly adsorbed in the free interface. As it gets crowded, unimers can backscatter to the bulk due to the non existence of a vacant site at the interface.

In the present manuscript we develop two approaches for the analysis of dynamic surface tension experiments from a pendant bubble tensiometer. The first approach concerns the diffusion length, where a finite l-value is considered in agreement with the experimental conditions in the literature[5]. We compare the classical spherical model ($l = +\infty$) with that obtained by taking into account a finite diffusion length. The last model has been performed for a one-dimensional system where the adsorption-desorption is considered to take place in a spherical bubble. Secondly, in order to take into consideration that the real geometry for a pendant bubble tensiometer resembles a distorted sphere, an axisymmetric model accounting for the experimental conditions has been developed. We compare numerical results with experimental dynamic surface tension ones obtained from the literature for a well known alkyl poly(ethylene oxide) surfactant, $C_{12}E_4$. Adsorption at the air-water interface of C_iE_j surfactants has been widely studied by different experimental techniques[5–16] concluding that for most of them the adsorption is diffusion-controlled.

Indeed, there are two general models that describe the adsorption into an interface[4]: the diffusion controlled model in which monomers adsorb directly because adsorption barriers are not taken into account, taking more time to travel from the bulk to the subsurface than the adsorption time, and the mixed-kinetic model, where monomers do not adsorb directly but have to overcome a potential barrier, proceed in the correct orientation or find an empty site to be adsorbed. Maldarelli et al.[13] probed the existence of a shift from the diffusion controlled model to the mixed-kinetic model for increasing bulk concentrations.

[a] *Department of Physical-Chemistry, Universidade de Vigo, Ourense, Spain.*
[b] *Department of Applied Mathematics I, Universidade de Vigo, Vigo, Spain.*
[c] *Department of Physical-Chemistry, Center for Research in Biological Chemistry and Molecular Materials (CIQUS), Universidade de Santiago, Santiago de Compostela, Spain. E-mail: luis.garcia@usc.es*
[d] *Department of Applied Mathematics, Universidade de Santiago, Santiago de Compostela, Spain.*
[e] *Department of Didactics of Experimental Sciences,Universidade de Santiago, Santiago de Compostela, Spain.*

2 Mathematical Modelling

In the 1940's Ward and Tordai[17] pioneered the mathematical description of the adsorption-desorption process[4] obtaining the well-known Ward and Tordai equation which gives an explicit relation between the interface and subsurface concentrations, both of them unknowns of the problem. Ward and Tordai[17] considered an infinite diffusion length, and many authors followed that assumption afterwards (see[18] for further reading), although it is an ideal consideration. Other authors[19–22] considered a finite diffusion length offering different approaches in order to estimate it. In the present work, we carry out an analysis in terms of both finite and infinite diffusion lengths.

Here, we denote by r the radial distance (see fig.1), and $c(r,t)$ the concentration of surfactant at point $r \in [b,B]$ and time $t \in [0,T]$. Moreover, we denote the surface concentration by $\Gamma(t)$. The model for the diffusion of surfactant relies on the Fick's law written for a spherical coordinate system:

$$\frac{\partial c}{\partial t}(r,t) = \frac{D}{r^2}\frac{\partial}{\partial r}\left(r^2\frac{\partial c}{\partial r}(r,t)\right) \qquad b < r < B, \quad t > 0, \quad (1)$$

with boundary conditions:

$$D\frac{\partial c}{\partial r}(b,t) = \frac{d\Gamma}{dt}(t) \qquad t > 0, \qquad (2)$$

$$c(B,t) = c_b \qquad t > 0, \qquad (3)$$

and initial conditions:

$$c(r,0) = c_b \qquad b < r \leq B, \qquad (4)$$

$$\Gamma(0) = 0, \quad c(b,0) = 0. \qquad (5)$$

Besides, D is the diffusion coefficient and c_b the bulk concentration. Note that $r = b$ represents the subsurface and $r = B$ a spherical interface far from the former, the diffusion length $l = B - b$, see fig. 1, being the distance from the subsurface at which the unimers behave as in the bulk. This parameter is of great importance because a longer diffusion length increases the time taken to reach equilibrium in this system, since the unimers have to diffuse a longer distance to be adsorbed.

Note that diffusion in the bulk of the solution is described by eq. (1), which is a simplification of the generalized diffusion equation[23] where no convection is considered in the bulk phase. In this study, we have taken into account surfactant solutions below the cmc (critical micelle concentration), therefore D in eq. (1) can be assumed constant. Boundary conditions are given by eqs. (2)-(3). The former describes the surfactant flux between the subsurface and the spherical air bubble interface, the direction of which can be either from the subsurface to the interface (adsorption) or viceversa (desorption)[23]; the latter boundary condition describes the fact that, during the process, the boundary $r = B$ is kept at a constant bulk concentration, c_b.

In terms of initial conditions, eq. (4) states that the bulk phase is initially at a constant concentration, c_b, whereas the interface and the subsurface are supposed to be empty and, as eqs. (5) state, both concentrations are zero at the beginning of the process.

In order to close the system (1)-(5), it is necessary to specify what kind of adsorption-desorption mechanism follows the process. A diffusion controlled model governed by the Frumkin adsorption isotherm is mainly used in the present work. Frumkin isotherm takes into account the interactions between the solute and the solvent, being appropriate for non-ionic surfactants and thus more realistic than the Langmuir isotherm. Frumkin isotherm is given by the following expression:

$$\Gamma = \Gamma_m \frac{c_s}{c_s + a\exp(K\frac{\Gamma}{\Gamma_m})}, \qquad (6)$$

where Γ_m is the maximum surface concentration, $c_s(t) = c(b,t)$ for positive t, a is the surfactant activity and K is the molecular interaction. The parameter a depends on the non-ideality of the monomer layer formed in the interface. The constant K shows if the surfactant has a cooperative or anticooperative behaviour. A negative K value would indicate cohesive intermolecular forces as the surface populates and therefore the desorption rate is reduced; on the other hand, a positive K value would indicate an anticooperative adsorption, hindering adsorption as the interface gets more covered. Besides, when K equals zero, a particular and remarkable case of the Frumkin equation is obtained: the Langmuir adsorption isotherm which is given by:

$$\Gamma = \Gamma_m \frac{c_s}{a + c_s}, \qquad (7)$$

where $a = 1/K_L$, K_L being the Langmuir constant. This assumption implies that there are neither interactions nor intermolecular forces between monomers and the solvent (modelled as a lattice). Thus all adsorption sites are equivalent and the probability of adsorption in a vacant site is independent of the neighbourhood occupancy.

In the present study, the Frumkin and Langmuir isotherms are going to be compared, to test if their use introduces significant improvements in the simulations.

If the solution is considered ideal, a concentration dependant surface equation of state can be obtained, yielding the following expressions for the Frumkin and Langmuir isotherms, respectively:

$$\gamma = \gamma_0 + \mathrm{n}RT\Gamma_m\left[\ln(1-\frac{\Gamma}{\Gamma_m}) - \frac{K}{2}\left(\frac{\Gamma}{\Gamma_m}\right)^2\right], \quad (8)$$

$$\gamma = \gamma_0 + \mathrm{n}RT\Gamma_m\ln(1-\frac{\Gamma}{\Gamma_m}), \quad (9)$$

where γ_0 is the surface tension of pure water, n a factor accounting for the adsorption of counter-ions[18] (equal to 1 as $C_{12}E_4$ is non-ionic), R the gas constant and T the temperature.

3 One dimensional diffusion-controlled model

The diffusion-controlled model considers that the timescale for equilibration of the interface and the subsurface is very fast compared to the timescale for diffusion, and the adsorption process is described by a thermodynamic adsorption isotherm[24]. In this study, the diffusion controlled model and both the Frumkin and Langmuir isotherms (see (6) and (7), respectively) have been employed. These two equations establish a nonlinear dependence between the interface and the subsurface concentrations. We compare the numerical simulations with the experimental dynamic surface tension data under three different considerations. Firstly, we use an infinite diffusion length in order to test the existence of convective currents manifested by "superdiffusive" adsorption kinetics. Under the assumption of infinite diffusive length we analyze the influence of the pendant bubble size by considering diameters in the proximity of the pendant bubble one. Finally, we introduce a finite diffusion length for the one-dimensional model and compare the numerical results with those obtained under the classical spherical method.

3.1 Classical spherical method

The classical spherical method describes the adsorption of surfactant molecules onto a freshly created air spherical bubble surface, in an infinite surfactant solution, by considering the case of one-dimensional diffusion. This simplification comes from assuming spherical symmetry in the diffusion process which takes place in the bulk of the solution. That is to say, the same behaviour is assumed in all radial directions, so it is only necessary to determine one of them to simulate what happens in the whole solution.

The model under consideration is established in eqs. (1) to (5) by taking $B = +\infty$. A solution for the surface concentration is calculated by using the Laplace transform technique, and the following expression, in terms of the unknown subsurface concentration, is obtained[5,17,25,26]:

$$\Gamma(t) = \frac{D}{b}[c_b t - \int_0^t c_s(\tau)d\tau] + \left(\frac{D}{\pi}\right)^{1/2}[2c_b t^{1/2} - \int_0^t \frac{c_s(t-\tau)}{\tau^{1/2}}d\tau]. \quad (10)$$

Besides, this equation is coupled with either Frumkin (6) or Langmuir (7) isotherms in order to obtain both surface and subsurface concentrations. Once they are known, the surface tension is calculated using the surface equations of state for the above isotherms (8) or (9), respectively.

Now we describe the numerical scheme implemented in MATLAB and we present several numerical results together with experimental data, taking into account the discretization of the Ward-Tordai expression (10), together with Frumkin (6) or Langmuir (7) equations. In order to do that, we use a uniform partition of the time interval $[0,T]$, denoted by $0 = t_0 < t_1 < \ldots < t_N = T$, with time step $k = T/N$ and nodes $t_n = nk$ for $n = 0,1,\ldots,N$. For a continuous function $z(t)$, we use the notation $z_n = z(t_n)$, $n = 0,1,\ldots,N$. So, the discrete approximation of this problem is considered as follows[27]:

Problem P^k. Find $\Gamma^k = \{\Gamma_n^k\}_{n=0}^N$ and $c_s^k = \{(c_s)_n^k\}_{n=0}^N$ such that

$$\Gamma_0^k = 0, \quad (c_s)_0^k = 0, \quad (11)$$

and, for $n = 1,\ldots,N$, Γ_n^k and $(c_s)_n^k$ are the solution to the following equations:

$$\Gamma_n^k = \Gamma_m\frac{(c_s)_n^k}{(c_s)_n^k + a\exp(K(\Gamma_n^k/\Gamma_m))}, \quad (12)$$

$$\Gamma_n^k = \frac{D}{b}[c_b t_n - \mathfrak{A}_n] + \left(\frac{D}{\pi}\right)^{1/2}[2c_b t_n^{1/2} - \mathfrak{B}_n], \quad (13)$$

$\mathfrak{A}_n$ and $\mathfrak{B}_n$ being expressions to approximate the integrals of eq. (10), obtained by means of a piecewise linear interpolation of the subsurface concentration, $c_s(t)$, on the discretization nodes of the time interval. So, both $\mathfrak{A}_n$ and $\mathfrak{B}_n$ depend on the concentrations $(c_s)_0^k, (c_s)_1^k, \ldots, (c_s)_n^k$ and are given by the following expressions[27]:

$$\mathfrak{A}_n = \frac{k}{2}\sum_{i=0}^{n-1}((c_s)_i^k + (c_s)_{i+1}^k),$$

and

$$\mathfrak{B}_n = \frac{4}{3}k^{1/2}(c_s)_n^k + \frac{2}{3}k^{1/2}(c_s)_{n-1}^k + 2k^{1/2}\sum_{i=1}^{n-1}\left[(c_s)_{n-i}^k\,\alpha_i + (\frac{1}{3}\theta_i - i\,\alpha_i)((c_s)_{n-i-1}^k - (c_s)_{n-i}^k)\right],$$

where $\alpha_i = (i+1)^{1/2} - i^{1/2}$ and $\theta_i = (i+1)^{3/2} - i^{3/2}$. Note that, at iteration n, the two unknowns of Problem P^k are Γ_n^k and $(c_s)_n^k$ assembled in a system of two equations and two unknowns, eq. (12) and eq. (13), being straightforwardly solved by substitution in the case of the Langmuir isotherm and by applying the Newton method for nonlinear systems (see[28]) if we consider the Frumkin model.

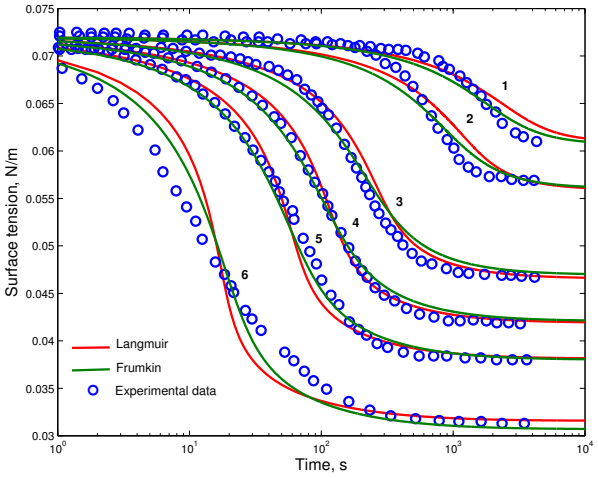

Fig. 2 Comparison of experimental surface tension data ○, reported in reference[5], with the numerical surface tension obtained with Langmuir (red curves) and Frumkin (green curves) models taking into account infinite diffusion length for different concentrations of $C_{12}E_4$ at 25.0°C ($\gamma_0 = 0.072$ N/m), $D = 6.4\times10^{-10}$ m^2/s. The model constants for the Langmuir isotherm are $\Gamma_m = 3.905\times10^{-6}$ mol/m^2, $a = 4.66\times10^{-4}$ mol/m^3 and $K = 0$ and for the Frumkin isotherm $\Gamma_m = 4.663\times10^{-6}$ mol/m^2, $a = 3.521\times10^{-4}$ mol/m^3 and $K = 1.875$. **Curve 1**: $c_b = 10^{-3}$ mol/m^3, **curve 2**: $c_b = 2\times10^{-3}$ mol/m^3 , **curve 3**: $c_b = 6\times10^{-3}$ mol/m^3, **curve 4**: $c_b = 10\times10^{-3}$ mol/m^3, **curve 5**: $c_b = 15\times10^{-3}$ mol/m^3, **curve 6**: $c_b = 30\times10^{-3}$ mol/m^3.

Numerical results for different $C_{12}E_4$ concentrations are shown in fig. 2 and are compared with the literature data taking into account a pendant bubble radius equal to $b = 1$ mm. It can be seen that the agreement between the simulations and the experimental data is quite good.

Fig. 2 shows that the predicted dynamic surface tension profiles match the experimentally observed behaviour at higher surfactant concentrations, while systematic deviations exist at lower ones (see curves 1 and 2 for $C_{12}E_4$). It should be noted that although the experimental and predicted dynamic surface tension profiles deviate at low surfactant concentrations, both the predicted and experimental behaviours approach the same equilibrium surface tension values. Consequently, the observed systematic deviations may not be associated with the equilibrium surfactant adsorption models. Blankschtein and coworkers[29] have showed kinetics of surfactant adsorption to be faster than the predicted faster rate of surfactant adsorption from a quiescent solution at time scales greater than 100s. In agreement with Blankschtein proposal[29], this finding suggests that the actual surfactant bulk solution, in which the pendant-bubble dynamic surface tension measurements were conducted, cannot be considered to be quiescent at time scales greater than 100s, suggesting the possible existence of convective currents operating at time scales greater than 100s in the surfactant bulk solution.

3.2 Influence of the bubble radius

Recent studies[22,30] in the literature reveal that the time scales for reaching the equilibrium for surfactants adsorption at the air-water interface change significantly with pendant bubble radius. Fig. 3 shows the numerical dynamic surface tension with different bubble radii by using the classical spherical method with infinite diffusion length and Frumkin isotherm. Pendant bubble radii values ($b = 0.01 - 10$ mm) have been chosen in the vicinity of the actual pendant bubble radius ($b = 1$ mm).

When the interface is curved, the characteristic time scale for molecular diffusion depends on the interface curvature. The ratio between the bubble surface area and the volume surrounding the bubble decreases with increasing radius. In other words, there are more molecules per unit area available for adsorption near a spherical interface with decreasing radii. This increases the rate of mass transfer to the sphere. According to the Laplace-Young equation, variations of the radius of the sphere have a direct effect in the difference of pressures between the inner and outer side of the bubble. If the radius decreases, the inner pressure of the bubble increases, and consequently the magnitude of adsorption grows. Indeed, this increase in the quantity of unimers adsorbed accelerates the process achieving the equilibrium faster.

The simulations of fig. 3 agree with the above mentioned. It is plain to see that, for smaller bubbles, the surface tension achieves equilibrium faster than for bigger ones, due to the rapid adsorption of unimers caused by the increase of the magnitude of adsorption, to compensate the increase of inner pressure of the bubble. Under the experimental conditions used in this study, the influence of the bubble radius, $b = 1$ mm, can be neglected.

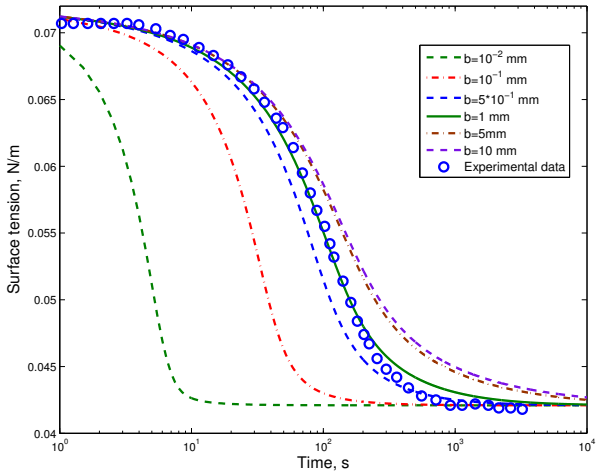

Fig. 3 Comparison of experimental surface tension data (○), taken from reference[5], with the numerical surface tension obtained varying surface of adsorption radius (Frumkin model and infinite length) for $C_{12}E_4$ at 25.0°C ($\gamma_0 = 0.072$ N/m), $D = 6.4 \times 10^{-10}$ m^2/s, $\Gamma_m = 4.663 \times 10^{-6}$ mol/m^2, $a = 3.521 \times 10^{-4}$ mol/m^3 with concentration $c_b = 10 \times 10^{-3}$ mol/m^3. Solid curve: $b = 1$ mm (green). Discontinuous curves: $b = 10^{-2}$ mm (**green**), $b = 10^{-1}$ mm (**red**), $b = 5 \times 10^{-1}$ mm (**blue**), $b = 5$ mm (**brown**), $b = 10$ mm (**purple**).

3.3 One-dimensional spherical model with finite diffusion length

The model presented in this section has been already introduced in eqs. (1) to (5), where a finite diffusion length is considered and adequately chosen in order to reproduce the bulk conditions[31]. We remark that B is the radius of an imaginary selected sphere, so that the amount of surfactant in the bulk phase is about 25-30 times greater than the amount of surfactant adsorbed onto the air bubble surface when the solution has reached the equilibrium. This way we guarantee that the bulk concentration does not change significantly with the migration of unimers to the interface, the amount of unimers adsorbed at the interface being negligible in agreement with Ward and Tordai. Fig. 4 depicts a sketch of the model.

The Frumkin isotherm is used here instead of Langmuir's due to its general extent, although in the present study the Frumkin isotherm does not offer any advantage over Langmuir's, probably because molecular interactions are not very significant.

The algorithm developed to obtain the numerical results with this model has been implemented in MATLAB and it is based on the finite element method, consisting of, roughly speaking, approximating the solution of the continuous problem considering finite dimensional vector spaces. This way the solution is calculated in a finite set of nodes of the domain and then a continuous approximate solution is built by interpolation.

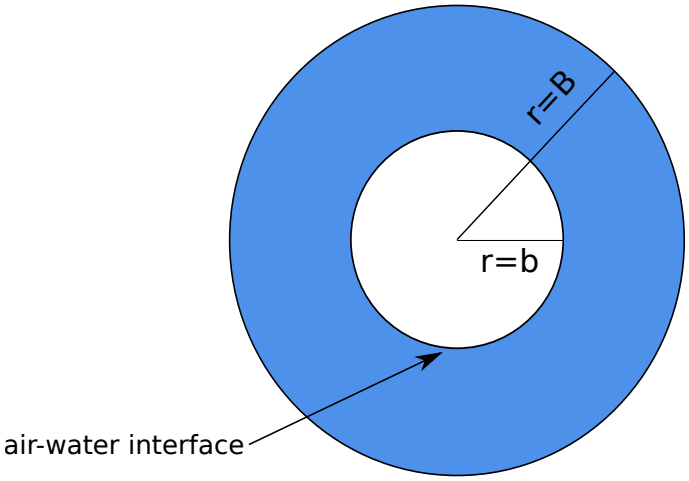

Fig. 4 Sketch of the diffusion region.

For the time discretization of eqs. (1) to (5) we consider an implicit Euler method over a uniform partition of the time interval $[0,T]$ — see the previous section —, approximating the time partial derivative of the concentration in eqs. (1) and (2) by the two-point backward finite difference formula:

$$\frac{\partial c}{\partial t}(r,t_n) \approx \frac{c_n(r) - c_{n-1}(r)}{k}.$$

In order to obtain the fully discrete approximation of this problem, we define a non-uniform partition of the spatial domain, the interval $[b,B]$, denoted by $b = a_0 < a_1 < \cdots < a_M = B$, with $h_i := a_{i+1} - a_i, i = 0,\ldots,M-1$.

Now we briefly describe the numerical scheme which has been performed to obtain the numerical results. We consider the finite element space V^h defined as follows:

$$V^h = \{v^h \in C([b,B]); v^h_{|[a_{i-1},a_i]} \in P_1([a_{i-1},a_i]), \\ i = 1,\ldots,M, v^h(B) = 0\},$$

where $P_1([a_{i-1},a_i])$ denotes the set of polynomials of degree less or equal to one in the interval $[a_{i-1},a_i], i = 1,\ldots,M$ and $h := \max_{0 \le i \le M-1} h_i$.

Therefore, for $n = 1,2,\ldots,N$, given $c^{hk}_{n-1} \in V^h$ and $\Gamma^{hk}_{n-1} \in \mathbb{R}$, the discrete concentration of surfactant, $c^{hk}_n + c_b$, is obtained by solving the following nonlinear problem:

$$\int_b^B r^2 c_n^{hk} v^h dr + Dk \int_b^B r^2 \frac{\partial c_n^{hk}}{\partial r} \frac{\partial v^h}{\partial r} dr + b^2 \frac{\Gamma_m \beta_{n-1}^{hk} (c_n^{hk}(b) - c_{n-1}^{hk}(b))}{(\beta_{n-1}^{hk} + c_n^{hk}(b) + c_b)^2 + K \beta_{n-1}^{hk} (c_n^{hk}(b) + c_b)} v^h(b) = \int_b^B r^2 c_{n-1}^{hk} v^h dr, \quad \forall v^h \in V^h,$$

where $\beta_{n-1}^{hk} = a \exp(K(\Gamma_{n-1}^{hk}/\Gamma_m))$.

To deal with the previous nonlinear problem, we have used an iterative algorithm based on a fixed-point argument at each time step. In what follows, we describe this algorithm, which solves a linear system in each iteration:

1. **Initial time step**. At the beginning, c_0^{hk} and Γ_0^{hk} are given.
2. **(n)th time step**. Both the surfactant and the surface concentrations at time t_{n-1}, c_{n-1}^{hk} and Γ_{n-1}^{hk}, respectively, are known. Then, at time t_n, c_n^{hk} is obtained with the following iterative algorithm:

   - Initialization: $\lambda_{n,0} = 1$. Then $c_{n,0}^{hk}$ is computed as the solution to the linear equation

   $$\int_b^B r^2 c_{n,0}^{hk} v^h dr + Dk \int_b^B r^2 \frac{\partial c_{n,0}^{hk}}{\partial r} \frac{\partial v^h}{\partial r} dr + b^2 \Gamma_m \beta_{n-1}^{hk} \lambda_{n,0} c_{n,0}^{hk}(b) v^h(b) = \int_b^B r^2 c_{n-1}^{hk} v^h dr + b^2 \Gamma_m \beta_{n-1}^{hk} \lambda_{n,0} c_{n-1}^{hk}(b) v^h(b), \quad \forall v^h \in V^h.$$

   - Iteration j: $c_{n,j-1}^{hk}$ is known. So, we successively calculate $\lambda_{n,j}$

   $$\lambda_{n,j}^{-1} = (\beta_{n-1}^{hk} + c_{n,j-1}^{hk} + c_b)^2 + K \beta_{n-1}^{hk} (c_{n,j-1}^{hk} + c_b),$$

   and determine $c_{n,j}^{hk}$ by solving the following linear system:

   $$\int_b^B r^2 c_{n,j}^{hk} v^h dr + Dk \int_b^B r^2 \frac{\partial c_{n,j}^{hk}}{\partial r} \frac{\partial v^h}{\partial r} dr + b^2 \Gamma_m \beta_{n-1}^{hk} \lambda_{n,j} c_n^{hk}(b) v^h(b) = \int_b^B r^2 c_{n-1}^{hk} v^h dr + b^2 \Gamma_m \beta_{n-1}^{hk} \lambda_{n,j} c_{n-1}^{hk}(b) v^h(b), \quad \forall v^h \in V^h.$$

   The algorithm stops if the following condition is fulfilled for a positive parameter ε small enough:

   $$\frac{|c_{n,j}^{hk} - c_{n,j-1}^{hk}|}{|c_{n,j-1}^{hk}|} < \varepsilon.$$

   Now, we know c_n^{hk} and then we can calculate Γ_n^{hk} by solving the following equation

   $$\Gamma_n^{hk} = \Gamma_m \frac{c_n^{hk}(b) + c_b}{\beta_{n-1}^{hk} + c_n^{hk}(b) + c_b}.$$

Once the bulk surfactant concentration is known, the surface tension is calculated by means of the Frumkin surface equation of state (8).

Now, we present the behaviour of this model for the simulation of different $C_{12}E_4$ solutions. First of all, we analyze the influence of the diffusion length on the dynamic surface tension relaxation. We have performed several simulations varying its value for a solution with concentration $c_b = 10 \times 10^{-3}$ mol/m^3, see fig. 5. Taking into account that the radius of the bubble, b, is equal to 1 mm, the diffusion length needed to simulate the infinite boundary condition is $B = 3.3$ mm. This value[31] is calculated so that the amount of surfactant in the volume between the two spheres is 30 times bigger than the amount of surfactant adsorbed onto the air bubble surface when the solution is at equilibrium. With diffusion lengths below this value, the curve falls faster, so equilibrium is reached before. On the other hand, considering values of the diffusion length greater than $B = 3.3$ mm provides similar results.

The decrease in the surface tension curves becomes sharper as we reduce the value of B, reaching the equilibrium surface tension faster than the experimental data. For diffusion lengths smaller than $B = 3.3$ mm the experimental results do not fit the numerical predictions, since in this case the numerical model does not describe tightly the experimental conditions; that is to say, for small values of B the number of unimers being adsorbed to the interface is not negligible compared to their number in the spherical volume under consideration.

Fig. 6 shows the relaxation profiles of the surface tension generated from the Frumkin and Langmuir models, by using the same diffusion coefficient ($D = 6.4 \times 10^{-10}$ m^2/s) and by considering the one-dimensional spherical model with finite diffusion length. Discrepancies between both models are in agreement with predictions from the literature[5,32–34], the Frumkin model being only slightly better than the Langmuir one. Because of its generality and the very small discrepancies, the Frumkin isotherm is chosen instead of Langmuir's to analyze the transfer from the subsurface to the air-water interface.

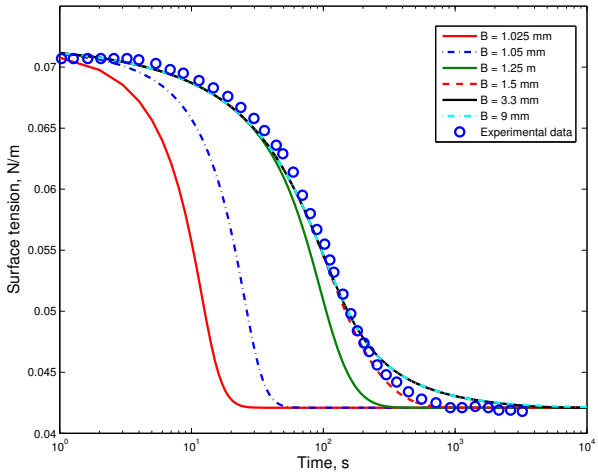

Fig. 5 Numerical surface tension calculated with Frumkin model for different diffusion lengths compared with experimental data taken from[5]. $C_{12}E_4$ at 25.0°C with concentration $c_b = 10\times10^{-3}$ mol/m^3 ($\gamma_0 = 0.072$ N/m), $D = 6.4\times10^{-10}$ m^2/s, $\Gamma_m = 4.663\times10^{-6}$ mol/m^2, $a = 3.521\times10^{-4}$ mol/m^3, $K = 1.875$. Curve ○: experimental data. Discontinuous curves: $B = 1.05$ mm (**blue**), $B = 1.5$ mm (**red**), $B = 9$ mm (**light blue**). Solid curves: $B = 1.025$ mm (**red**), $B = 1.25$ mm (**green**), $B = 3.3$ mm (**black**).

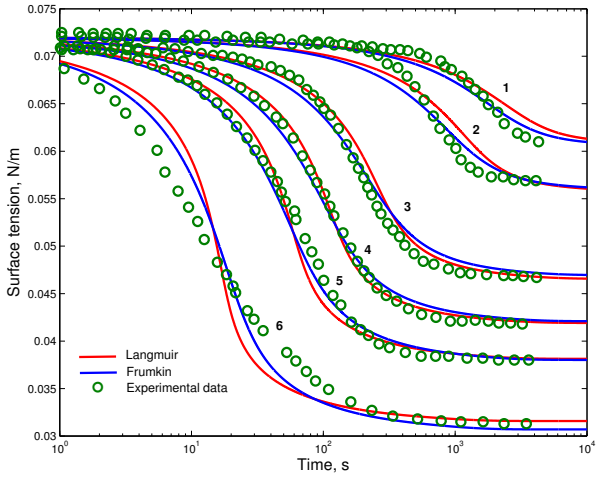

Fig. 6 Comparison of experimental dynamic surface tension data, taken from[5], for $C_{12}E_4$ at 25.0°C and predictions from the Frumkin (blue lines) and Langmuir (red lines) isotherms. $\gamma_0 = 0.072$ N/m; $D = 6.4\times10^{-10}$ m^2/s. Frumkin isotherm: $\Gamma_m = 4.663\times10^{-6}$ mol/m^2; $a = 3.521\times10^{-4}$ mol/m^3 and $K = 1.875$. Langmuir isotherm: $\Gamma_m = 3.905\times10^{-6}$ mol/m^2 and $a = 4.66\times10^{-4}$ mol/m^3, $K = 0$. Curve 1 ($c_b = 1\times10^{-3}$ mol/m^3; $B = 6.22$ mm), curve 2 ($c_b = 2\times10^{-3}$ mol/m^3; $B = 5.24$ mm), curve 3 ($c_b = 6\times10^{-3}$ mol/m^3; $B = 3.81$ mm), curve 4 ($c_b = 10\times10^{-3}$ mol/m^3; $B = 3.30$ mm), curve 5 ($c_b = 15\times10^{-3}$ mol/m^3; $B = 2.87$ mm), curve 6 ($c_b = 30\times10^{-3}$ mol/m^3; $B = 2.32$ mm).

4 Axisymmetric model with finite diffusion length

In this section, we work with an axisymmetric model considering two different geometries. In the first one, the adsorption takes place onto a spherical bubble hanging from the tip of the inverted needle inside the solution. However, in order to be more realistic and reproduce the real situation of the pendant bubble tensiometer, we deal with a second geometry in which adsorption occurs onto a non perfect sphere but onto a deformed bubble due to the gravity force.

In order to get the shape of the non spherical pendant bubble we use the Laplace-Young equation given by the following expression

$$\gamma_{eq}\, 2H + \rho\, g\, h = C^\star,$$

where γ_{eq} is the surface tension at equilibrium, H the surface mean curvature, ρ the density, g the gravitational acceleration, h the height with respect to the reference position (see fig. 7) and $C^\star$ denotes a real constant accounting for the pressure difference. Thus, the bubble shape is determined by a static balance between surface tension and gravitational forces.

In order to compute the free boundary a system of cylindrical coordinates is used with the $z-$axis coinciding with the symmetry axis of the bubble as it is depicted in fig. 7. We assume that the bubble can be obtained as a surface of revolution by rotating the curve $r = s(z)$ about the $z-$axis. Taking into account the unit normal vector to this surface, $\mathbf{n}$, and since $2H = -\nabla\cdot\mathbf{n}$ (see[35]) the Laplace-Young equation can be rewritten as follows

$$\gamma_{eq}\,\frac{1+(s'(z))^2 - s(z)s''(z)}{s(z)(1+(s'(z))^2)^{3/2}} + \rho\, g(b-z) = C^\star, \qquad (14)$$

b being the radius of the spherical bubble.

In order to avoid the values where r is zero, we calculate the deformed bubble from the point P_0 —see fig. 7—, assuming that at this point the bubble is spherical to obtain the value of the constant $C^\star$. Notice that the expression (14) is a second-order ordinary differential equation which can be solved as a system of two first-order ordinary differential equations:

$$y_1'(z) = y_2(z),$$
$$y_2'(z) = \frac{1+(y_2(z))^2}{y_1(z)} + \frac{d\,\rho\, g(b-z) - C^\star d}{\gamma_{eq} y_1(z)},$$

where $y_1(z) = s(z)$, $d = y_1(z)(1+y_2(z)^2)^{3/2}$ and the initial conditions are given by

$$y_1(z_0) = s(z_0) = r_0,$$
$$y_2(z_0) = s'(z_0) = \frac{-z_0}{(b^2 - z_0^2)^{1/2}}.$$

The solution of the previous system is obtained by means of the MATLAB function ODE45. In fig. 8 the shape of

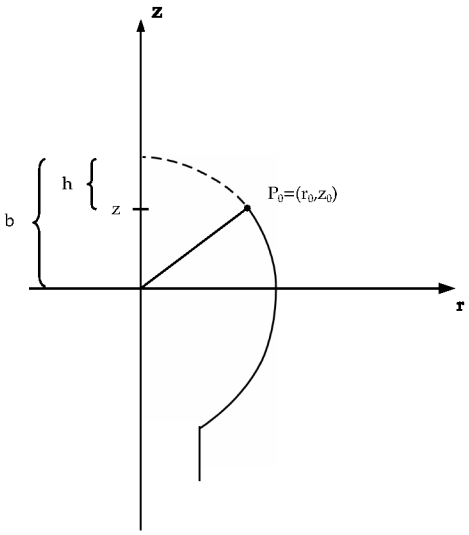

Fig. 7 Coordinate system and shape of the deformed bubble.

the spherical bubble (green curve) is shown together with the shape of the bubbles obtained for different concentrations. In order to obtain the shape of the non spherical bubbles, we take $\rho = 997.019$ kg/m^3 and the surface tension at equilibrium is computed using equation (9).

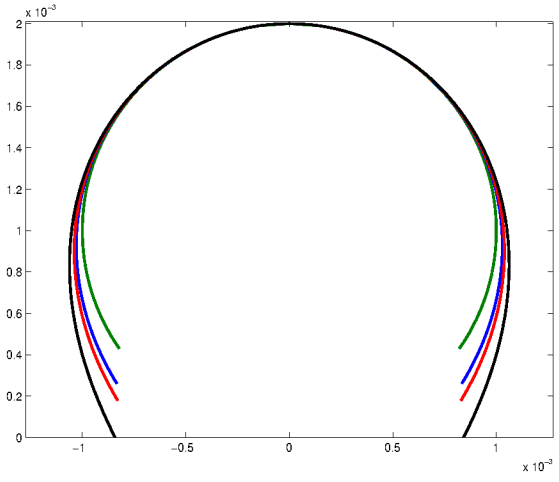

Fig. 8 Shape of the different bubbles considered in the axisymmetric model. Spherical bubble (green curve). Non spherical bubbles for concentrations $c_b = 10^{-3}$ mol/m^3 (blue curve), $c_b = 6\times10^{-3}$ mol/m^3 (red curve) and $c_b = 30\times10^{-3}$ mol/m^3 (black curve).

The approximations of the diffusion-controlled model explained in previous sections consider that adsorption takes place in the whole surface of an spherical air bubble. In order to analyze if this fact plays a major role on the prediction of the dynamic surface tension, we have taken into account an axisymmetric model assuming cylindrical symmetry and the fact that the concentration does not depend on the angular coordinate. Therefore, in this section the time-dependent concentration around the bubble tensiometer is numerically computed exploiting its axial symmetry. Indeed, hereafter Ω denotes a radial section of the bulk, depicted in fig. 9, for both spherical bubble (left) and distorted bubble (right); the radius of the spherical bubble is 1 mm and the needle radius is $r_c = 0.825$ mm in both domains. For the boundary notation, the first subscript $i = 1$ denotes the spherical case and $i = 2$ stands for the distorted case, the boundary of Ω being the union of the following sets:

- $\Gamma_{i,1}$: Subsurface bubble ($i = 1,2$).
- $\Gamma_{i,2}$: An artificial boundary limiting the bulk suitably picked to simulate the bulk conditions (following the same criteria as in the previous model) ($i = 1,2$).
- $\Gamma_{i,3}$: Air-water interface ($i = 1,2$).
- $\Gamma_{i,4}$: Wall of the needle ($i = 1,2$).
- Γ_S: Symmetry boundary.

This axisymmetric setting leads to a diffusion problem in which the adsorption takes place onto the boundary $\Gamma_{i,1}$, $i = 1,2$. Besides, the following system of equations establishes this model in cylindrical coordinates:

$$\frac{\partial c}{\partial t} - \frac{1}{r}\frac{\partial}{\partial r}\left(rD\frac{\partial c}{\partial r}\right) - \frac{\partial}{\partial z}\left(D\frac{\partial c}{\partial z}\right) = 0, \text{ in } \Omega\times(0,T), \quad (15)$$

with boundary conditions:

$$D\frac{\partial c}{\partial \mathbf{n}} = -\frac{d\Gamma}{dt} \quad \text{on} \quad \Gamma_{i,1},\ t>0, \quad (16)$$

$$c = c_b \quad \text{on} \quad \Gamma_{i,2},\ t>0, \quad (17)$$

$$D\frac{\partial c}{\partial \mathbf{n}} = 0 \quad \text{on} \quad \Gamma_{i,3}\cup\Gamma_{i,4}\cup\Gamma_S,\ t>0, \quad (18)$$

and initial conditions:

$$c = c_b \quad \text{in} \quad \Omega,\ t=0, \quad (19)$$

$$\Gamma = 0, c = 0 \quad \text{on} \quad \Gamma_{i,1},\ t=0, \quad (20)$$

$i = 1,2$, where $\mathbf{n}$ is the outward unit normal vector to the boundary. We remark that, in order to reproduce the physical setting, the adsorption surface consists of either a sphere

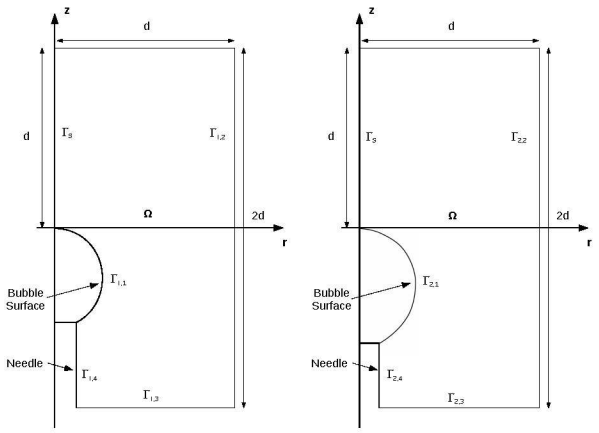

Fig. 9 Coordinate system and domain for the axisymmetric setting with classical spherical (left) and distorted pendant bubble (right).

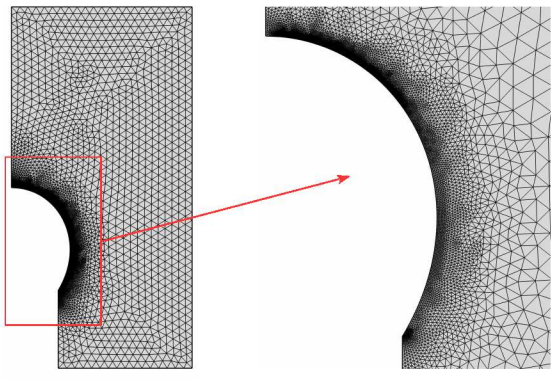

Fig. 10 Mesh and detail of the bubble boundary.

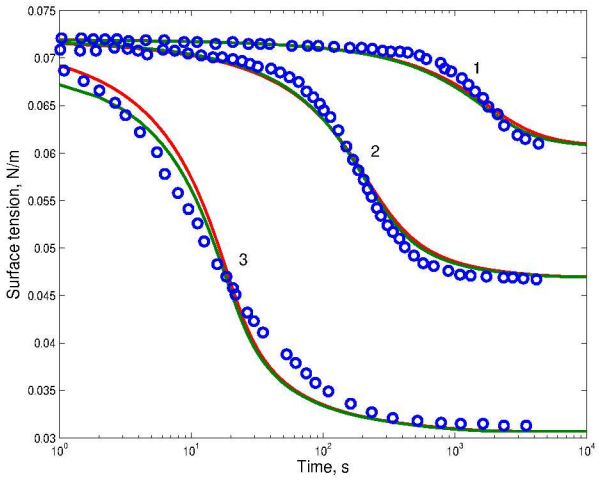

Fig. 11 Comparison of the experimental surface tension taken from reference[5] with the numerical surface tension calculated with the one-dimensional model with finite diffusion length (red lines) and with axisymmetric model taking a spherical bubble (green lines) for different concentrations of $C_{12}E_4$ at 25.0°C ($\gamma_0 = 0.072$ N/m), $D = 6.4 \times 10^{-10}$ m^2/s, $\Gamma_m = 4.663 \times 10^{-6}$ mol/m^2, $a = 3.521 \times 10^{-4}$ mol/m^3, $K = 1.875$. **Curve 1:** $c_b = 10^{-3}$ mol/m^3, **curve 2:** $c_b = 6 \times 10^{-3}$ mol/m^3, **curve 3:** $c_b = 30 \times 10^{-3}$ mol/m^3.

or a distorted sphere. Furthermore, the boundary condition eq. (18), imposed on $\Gamma_{i,3}$ and $\Gamma_{i,4}$, $i = 1, 2$, indicates that there is no molecular flux on those boundaries.

Finally, in order to close the problem, we consider the Frumkin isotherm, eq. (6), coupled with the model by means of boundary condition (16).

Numerically, we have solved this problem employing the finite element code COMSOL Multiphysics using Lagrange $\mathbb{P}_2$ elements. In order to validate the model, the mesh independence of the results is checked by computing the solution on several successively refined meshes, all of them having the same particularity: the smallest elements are located in the area of maximum curvature, that is to say, in the neighbourhood of the air bubble (see fig. 10). Note that in this model both the subsurface and surface concentrations depend on the spatial position. Thus, the average subsurface concentration is computed upon the bubble surface profile, and then this data is used into eq. (8) to find its average surface tension.

Fig. 11 shows a comparison of the experimental surface tension taken from reference[5] with the numerical surface tension calculated with the one-dimensional model with finite diffusion length (red lines) and with axisymmetric model taking a spherical bubble subsurface (green lines) for different concentrations of $C_{12}E_4$ at 25.0°C. As can be seen, both models are in good agreement for low concentrations being the largest deviations associated to high concentrations. On the other hand, in fig. 12 we present a comparison of the experimental surface tension taken from reference[5] with the numerical surface tension calculated with the axisymmetric model for a solution of $C_{12}E_4$ at 25.0°C for three concentrations considering a spherical bubble (green lines) and the distorted ones (red lines) depicted in fig. 8 for those concentrations. As can be seen, the introduction of the distorted bubbles does not provide any improvement in the results being quite similar to those obtained with the spherical bubble.

Figure 13 shows the comparison of experimental dynamic surface tension[5] with the calculated one by considering different approaches under the diffusion-controlled adsorption mechanism. In order to obtain the shape of the non spherical

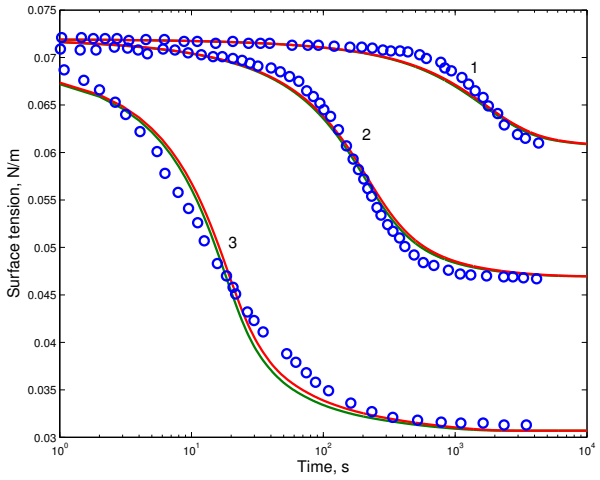

Fig. 12 Comparison of the experimental surface tension taken from reference[5] with the numerical surface tension calculated with the axisymmetric model for a solution of $C_{12}E_4$ at 25.0°C ($\gamma_0 = 0.072$ N/m), $D = 6.4 \times 10^{-10}$ m^2/s, $\Gamma_m = 4.663 \times 10^{-6}$ mol/m^2, $a = 3.521 \times 10^{-4}$ mol/m^3, $K = 1.875$. We compare the results obtained by considering that adsorption takes place onto the spherical bubble (green lines) and non spherical ones (red lines) depicted in figure 8 for the different concentrations.**Curve 1:** $c_b = 10^{-3}$ mol/m^3, **curve 2:** $c_b = 6 \times 10^{-3}$ mol/m^3, **curve 3:** $c_b = 30 \times 10^{-3}$ mol/m^3.

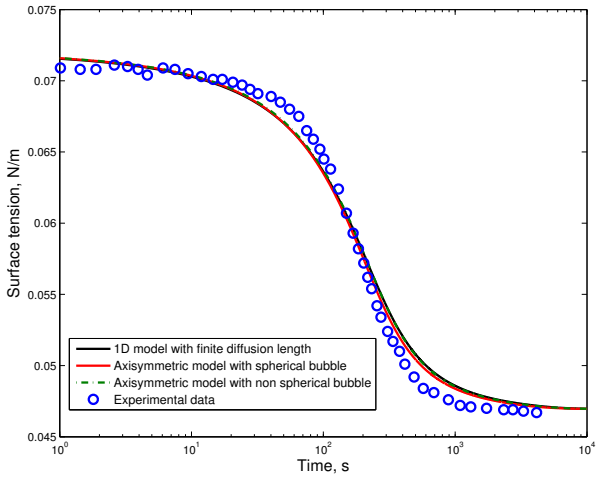

Fig. 13 Comparison of the experimental surface tension taken from[5] with the numerical surface tension calculated with the different models for a solution of $C_{12}E_4$ at 25.0°C with concentration $c_b = 6 \times 10^{-3}$ mol/m^3 ($\gamma_0 = 0.072$ N/m), $D = 6.4 \times 10^{-10}$ m^2/s, $\Gamma_m = 4.663 \times 10^{-6}$ mol/m^2, $a = 3.521 \times 10^{-4}$ mol/m^3, $K = 1.875$. B-value for the 1-D model is B=3.81mm.

bubble, we take $\rho = 997.019$ kg/m^3 and the surface tension at equilibrium for concentration $c_b = 6 \times 10^{-3}$ mol/m^3 is computed using equation (9) to get $\gamma_{eq} = 0.0466$ N/m. Axisymmetric models with both spherical and non-spherical bubbles yield almost equal numerical results. This is a consequence of the fact that small changes in curvature provide almost negligible effects on the adsorption rate supporting the accuracy of the 1D diffusion model.

Finally, in fig. 14 we present the evolution in time of the numerical surfactant concentration for a solution with bulk concentration $c_b = 6 \times 10^{-3}$ mol/m^3 at $t = 10$ s —fig. 14(a)—, $t = 100$ s —fig. 14(b)—, $t = 500$ s —fig. 14(c)— and $t = 1000$ s —fig. 14(d)—. Note that the range of the color scale varies at those pictures. It can be seen that surfactant molecules fill the air/water bubble surface until the solution becomes homogeneous. At $t = 1000$ s, the system has reached the equilibrium and so the concentration is nearly uniform in the bulk.

5 Conclusions

The main conclusions reached in this manuscript are related to the numerical simulation predictions of dynamic surface tension under consideration of a diffusion-controlled adsorption mechanism. We have compared the classical spherical method that considers an infinite diffusion domain with 1D and axisymmetric models on the assumption of a more physical realistic finite diffusion domain.

In order to achieve a more detailed description of the physical experiment, a finite diffusion domain has been considered through 1D and axisymmetric models. The dimensions of the diffusion domain were fixed to keep constant the surfactant concentration in this region. That is to say, the number of surfactant unimers in the diffusion domain should remain constant independently of its adsorption. Consequently, the dimensions of this domain depend both on the surfactant concentration and the size of the air-water interface. The results obtained with both 1D and axisymmetric models agree with those from the classical spherical model, being the main advantage the size of the domain.

6 Acknowledgements

This work has been partly supported by Xunta de Galicia under research projects PGIDIT 10PXIB291088PR, PGIDIT10-PXIB209113PR and 2007/085; and by Ministerio de Economía y Competitividad under research projects CTQ2011-22436 and MTM2012-36452-C02-02.

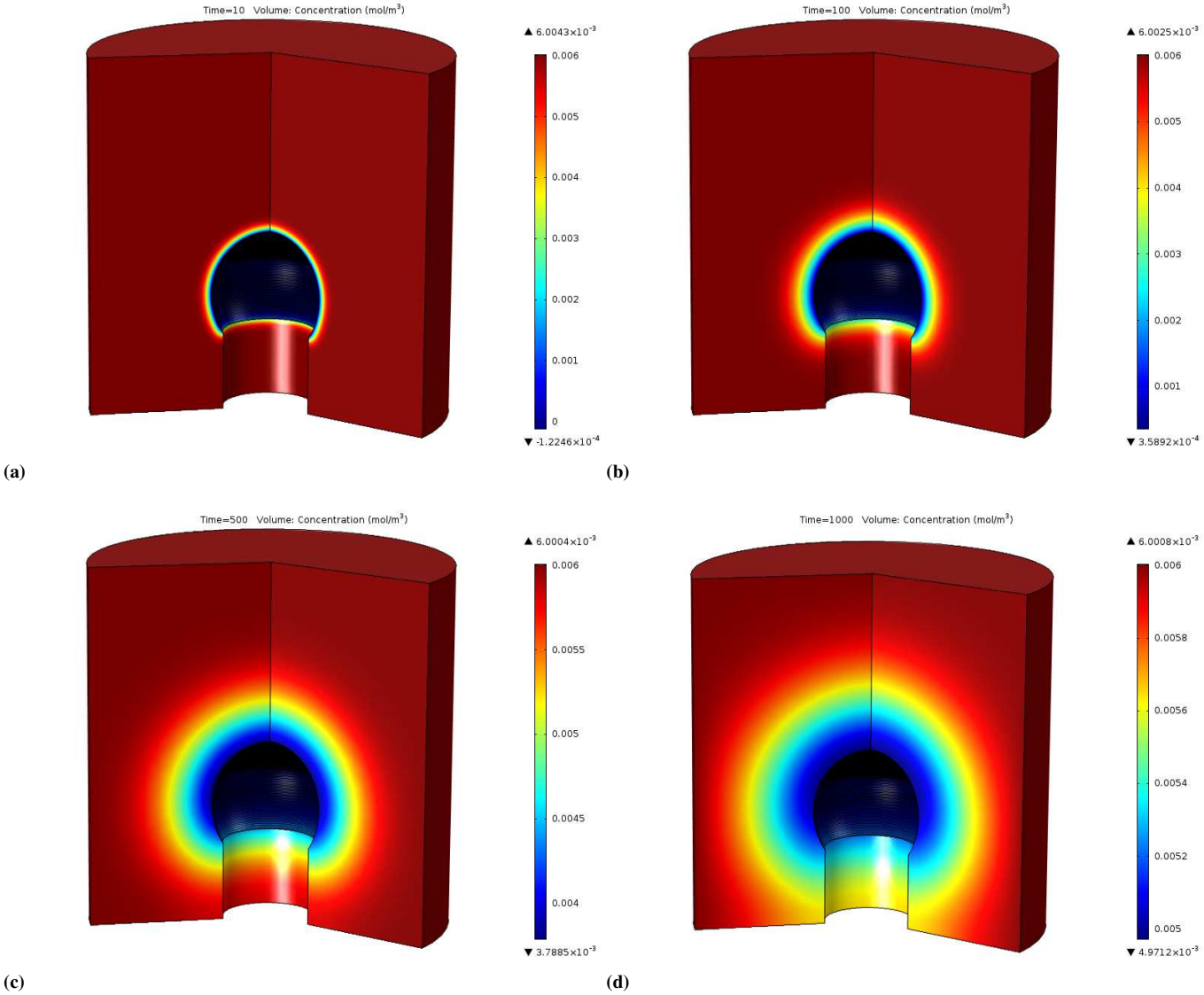

Fig. 14 Evolution of the distribution of unimers concentration at different times (in seconds) for a solution with bulk concentration $c_b = 6 \times 10^{-3}$ mol/m^3. 3D views of the axisymmetric numerical results. Note that the range of the color scale varies at those pictures.

References

1 A. W. Adamson and A. P. Gast, *Physical Chemistry of Surfaces*, Wiley, New York, 6th edn, 1997.
2 S. S. Dukhin, G. Kretzchmar and B. Miller, *Dynamics of adsorption at liquid interfaces*, Elsevier, Amsterdam, 1st edn, 1995.
3 M. J. Rosen, *Surfactants and interfacial phenomena*, Wiley, New Jersey, 3rd edn, 2004.
4 J. Eastoe and J. S. Dalton, *Adv. Colloid Interface Sci.*, 2000, **85**, 103–144.
5 C. T. Hsu, M. J. Shao and S. Y. Lin, *Langmuir*, 2000, **16**, 3187–3194.
6 J. Eastoe, J. S. Dalton, P. G. A. Rogueda, E. R. Crooks, A. R. Pitt and E. A. Simister, *J. Colloid Interface Sci.*, 1997, **188**, 423–430.
7 M. Ferrari, L. Liggerieri and F. Ravera, *J. Phys. Chem. B*, 1998, **102**, 10521–10527.
8 R. L. Bendure, *J. Coll. Interface Sci.*, 1971, **35**, 238–248.
9 P. Joos and E. Rillaerts, *J. Coll. Interface Sci.*, 1980, **79**, 96–100.
10 L. Liggieri, M. Ferrari, A. Massa, F. Francesca and F. Ravera, *Colloid Surf. A*, 1999, **156**, 455–463.
11 C. H. Chang, C. T. Hsu and S. Y. Lin, *Langmuir*, 1998, **14**, 2476–2484.
12 C. T. Hsu, M. J. Shao, Y. C. Lee and S. Y. Lin, *Langmuir*, 2000, **16**, 4846–4852.
13 R. Pan, J. Green and C. Maldarelli, *J. Coll. Interface Sci.*, 1998, **205**, 213–230.
14 S. Y. Lin, R. Y. Tsay, L. W. Lin and S. I. Chen, *Langmuir*, 1996, **12**, 6530–6536.
15 R. Miller, E. V. Aksenenko, L. Liggerieri, F. Ravera, M. Ferrari and V. B. Fainerman, *Langmuir*, 1999, **15**, 1328–1336.
16 J. Benjamins, A. Cagna and E. H. Lucassen-Reynders, *Coll. Surf. A*, 1996, **114**, 245.
17 A. F. H. Ward and L. Tordai, *J. Chem. Phys.*, 1946, **14**, 453–461.
18 C. H. Chang and E. I. Franses, *Colloid Surf.*, 1994, **100**, 1–45.
19 Y.-C. Lee, H.-S. Liu and S.-Y. Lin, *Colloid Surf. A*, 2003, **212**, 123–134.
20 C.-H. Chang, N.-H. L. Wang and E. I. Franses, *Colloids Surfaces*, 1992, **62**, 321–332.
21 K. J. Mysels, *J. Phys. Chem.*, 1982, **86**, 4648–4651.
22 N. J. Alvarez, L. M. Walker and S. L. Anna, *Phys. Rev. E*, 2010, **82**, 1–8.
23 R. Miller, P. Joos and V. B. Fainerman, *Adv. Colloid Interface Sci.*, 1994, **49**, 249–302.
24 J. R. Fernández and M. C. Muñiz, *Journal of Mathematical Chemistry*, 2011, **49**, 1624–1645.
25 H. S. Carslaw and J. C. Jaeger, *Conduction of Heat in Solids*, Oxford University Press, 1959.
26 M. R. Spiegel, *Laplace Transforms*, McGraw-Hill, 1965.
27 S.-Y. Lin, T.-L. Lu and W.-B. Hwang, *Langmuir*, 1995, **11**, 555–562.
28 F. S. A. Quarteroni, *Scientific Computing with MATLAB and Octave*, Springer-Verlag Italia, Milano, 2006.
29 S. N. Mookhanikkara and Blankschtein, *Langmuir*, 2009, **25**, 1434–1444.
30 N. J. Alvarez, L. M. Walker and S. L. Anna, *Langmuir*, 2010, **26**, 13310–13319.
31 M.-W. Yang, H.-H. Wei and S.-Y. Lin, *Langmuir*, 2007, **23**, 12606–12616.
32 C.-T. Hsu, C.-H. Chang and S.-Y. Lin, *Langmuir*, 1997, **13**, 6204–6210.
33 Y. C. Lee, S. Y. Lin and H. S. Liu, *Langmuir*, 2001, **17**, 6196–6202.
34 Y.-C. Lee, Y.-B. Liou, R. Miller, H.-S. Liu and S.-Y. Lin, *Langmuir*, 2002, **18**, 2686–2692.
35 N. T. Trudinger and D. Gilbarg, *Elliptic Partial Differential Equations of Second Order*, Springer- Verlag, Berlin, 1983.

7 Graphical Abstract

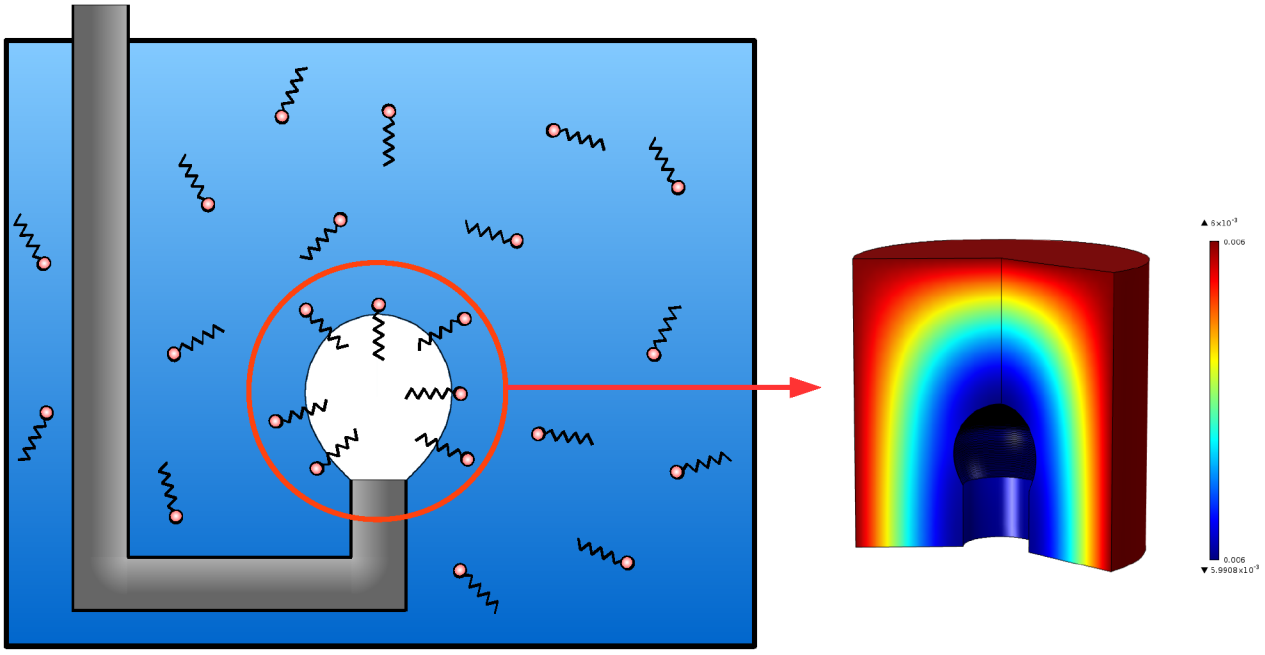

An axysimmetric model accounts for dynamic surface tension of non-ionic surfactants under consideration of diffusive adsorption behaviour with a finite diffusion length.